Elastic Wave Bandgaps in Origami-Based Periodic Strip Structures: A Computational Study

Soshun Ishihara and Shiro Biwa

Department of Aeronautics and Astronautics, Graduate School of Engineering, Kyoto University, Katsura, Nishikyo-ku, Kyoto 615-8540, Japan. E-mail: biwa@kuaero.kyoto-u.ac.jp

(Received 21 June 2025; accepted 01 November 2025)

The elastic wave bandgap characteristics of origami-based periodic strip-like waveguide structures are studied computationally. The computational models of waveguide structures are constructed by unidirectionally connecting unit cells composed of elastic plates according to Miura-ori or Jabara-ori (accordion fold) patterns, with the crease lines replaced by elastic interphase regions of finite width and thickness. The dispersion relations of these periodic structures are obtained by the finite element analysis based on the plate theory, and the elastic wave bandgaps lying at relatively low frequencies are identified. The results show that the location and width of the bandgaps depend significantly on the folding state of the structures, confirming their potential applicability as tunable acoustic metamaterials. The folding-state dependence of the bandgaps is shown for different parameters of the crease interphase regions and is discussed in light of unit-cell vibration modes at the bandgap edges. Furthermore, the wave transmission characteristics in the structures consisting of a finite number of unit cells are examined in relation to the bandgaps and the vibration modes of the corresponding periodic structures.

1. INTRODUCTION

Acoustic metamaterials are artificially designed media with periodic or nonperiodic microstructures and resonating elements that have untraditional characteristics of acoustic or elastic wave propagation.[1–3] Their unique properties are usually exhibited in the frequency range determined by their microstructural size or by the properties of the resonating elements. As a consequence, it is normal that acoustic metamaterials demonstrate maximal performance in specific ranges of frequency or wavelength. From a practical point of view, however, the tunability of the performance is desired in order to achieve suitable performance for variable external conditions.[4]

Recently, elastic waveguide structures based on the tessellation patterns of origami, which is originally a Japanese traditional art of paper folding, have been attracting active attention for their potential applications as tunable acoustic metamaterials owing to their foldable/deployable nature.[5,6] In order to exploit the waveguiding tunability of such origami-based structures, their wave propagation characteristics have been investigated using different analytical models. For example, bar-hinge or truss models[7] have been employed by Pratapa et al.[8,9] and Han et al.[10] to analyze the wave propagation and bandgap characteristics in origami-based structures of complex geometries. Beam models have also been used by Nanda and Karami[11] and Xu et al.[12] to analyze the flexural wave propagation and their bandgaps in zig-zag-shaped structures.

Although the bar and beam models used in the foregoing works[8–12] have successfully elucidated the bandgap properties of origami-based waveguide structures to a considerable degree, they have certain limitations in modeling the deformation behavior of sheet panels constituting the actual origami structures. In this respect, a two-dimensional plate modeling is an alternative candidate to analyze this issue. It is thus the aim of the present study to explore the elastic wave bandgap features of origami-based waveguide structures by modeling them as compositions of thin elastic plates and analyzing the dispersion relations by the finite element method. In order to illuminate the essential features of such structures, unidirectional strip-like structures constructed by unidirectionally connecting the unit cells of two kinds of origami tessellation patterns, i.e, Miura-ori and Jabara-ori (accordion fold), are considered. For these strip structures, our preliminary analysis[13] has shown that the bandgap features depend on their folding states significantly. In this paper, the variation of the elastic wave dispersion relations and the bandgap characteristics with their folding states are analyzed in more details. Furthermore, by taking advantage of the present plate-theory modeling, particular attention is paid to the panel deformation behavior associated with the vibration modes of the structures which was not thoroughly examined in the foregoing works based on the bar and beam models.

This paper is structured as follows. In Section 2, the computational models of the origami-based strip-like waveguide structures are introduced. In Section 3, the numerical procedures are outlined for the wave dispersion relations in the perfectly periodic structures and the wave transmission characteristics across the corresponding finite structures. The numerical results are shown and discussed in Section 4. The findings of the present study and aspects for further studies are summarized in Section 5.

2. MODELING OF ORIGAMI STRUCTURES

2.1. Miura-Ori Structure

Miura-ori[14] is an origami made of periodic crease patterns whose unit cell is a composite of four geometrically similar parallelograms. In Fig. 1(a), its fully deployed plane state is shown in the x-y plane, where a and b denote the length of the edges of each parallelogram and α denotes the angle between the edges. In this study, origami-based strip structures made by connecting the unit cells of Miura-ori unidirectionally along the x axis are considered. In order to give the waveguiding capability to the structures considered, the parallelograms, which are planes of null thickness in ideal origami, are replaced by flat elastic sheets with a nonzero thickness h. Furthermore, the crease lines are also replaced by elastic interphase regions with the same thickness h and a finite width s in line with our preliminary analysis.[13] It is noted that the idea of replacing the crease lines by elastic materials has also been shown by Han et al.[15] in their recent analysis of dynamic configuration transformation of an earwig-inspired origami structure. The crease interphase regions are assumed to be perfectly bonded to the neighboring panels over their entire boundaries so that the displacement and the rotation are continuous. In spite of this rigid bonding, the interphase regions themselves can represent various panel-panel connections such as adhesive layers, mechanical hinges, etc., through their equivalent stiffnesses when different material parameters are assigned. A schematic representation of a resulting Miura-ori structure and its unit cell are shown in Fig. 1(b) and Fig. 1(c), respectively. The dimensions of the unit cell in any folding states can be expressed in terms of a single parameter, i.e., the angle θ between each parallelogram and the x-y plane as shown in Fig. 1(b), which is called the folding angle hereafter. Taking into account the finite width of the crease interphase regions, the spatial period L of this structure in the x direction is given by:

$$L = 2b\frac{\tan\alpha\cos\theta}{\sqrt{1+\tan^2\alpha\cos^2\theta}} + 2s. \tag{1}$$

It is noted that a similar Miura-ori-based strip structure has been considered by Pratapa et al.[9] based on a bar-hinge model as one of their analytical examples.

2.2. Jabara-Ori Structure

In addition to the Miura-ori structure, an origami-based structure of simpler geometry is also considered in the present study, which consists of parallel and alternating mountain and valley creases as shown in Fig. 2(a), where the x axis is taken perpendicular to the crease lines. The distance of the neighboring mountain and valley creases are denoted by d. Based on this folding pattern, an origami-based strip structure is considered by connecting the unit cells consisting of two rectangles with the edge lengths c and d in the x direction. In this paper, this is referred to as the Jabara-ori structure in accordance with the common terminology in Japanese origami community, while this pattern is popularly known as accordion fold. A schematic of the resulting structure and its unit cell are shown in Fig. 2(b) and Fig. 2(c), respectively. Similarly to the Miura-ori structure defined above, the rectangles and the crease lines are modeled as flat sheets and interphase regions of the thickness h and the interphase width s, respectively. The spatial period of this structure in the x direction is given by:

$$L = 2d\cos\theta + 2s. \tag{2}$$

Similar zig-zag-shaped structures have been considered by Nanda and Karami[11] and Xu et al.[12] based on beam theories.

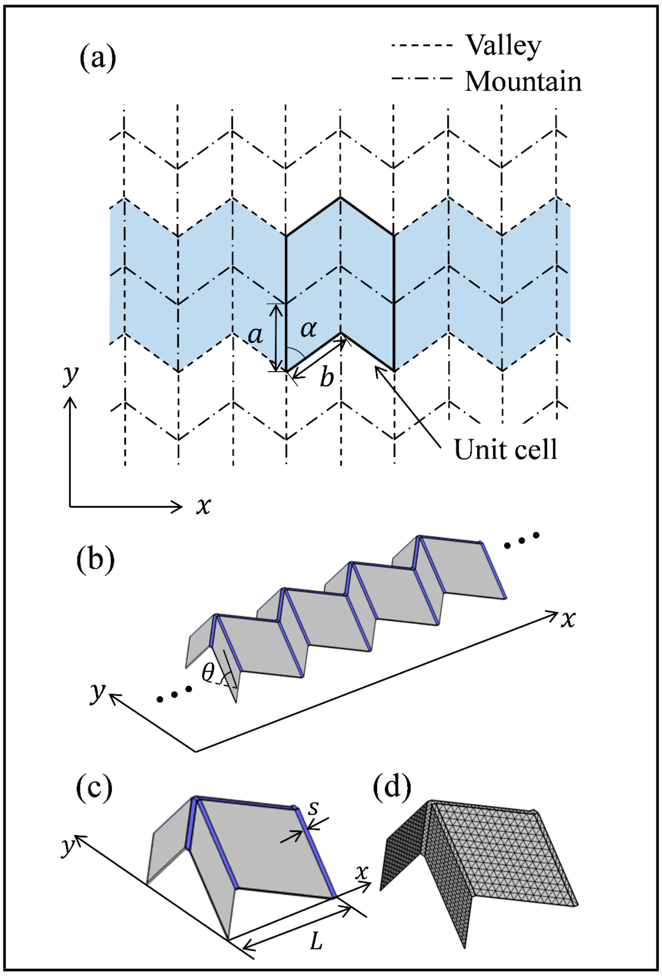

Figure 1. The schematics of (a) the folding pattern of Miura-ori, (b) the strip-like waveguide structure considered in this study, (c) its unit cell and (d) the finite element model.

3. NUMERICAL ANALYSIS

3.1. Analysis of Dispersion Relation

The dispersion relation of elastic waves in periodic structures can be obtained by the so-called Bloch wave analysis which characterizes the wave modes allowed to propagate in such structures. Since the theoretical framework for this analysis has been documented in many references,[16] only its outline is given here. In this analysis, the time-harmonic motion in the absence of external forces is considered for a unit cell of the periodic structure. When the time-harmonic displacement field in the unit cell is analyzed by the finite element method, the governing equations take the form $\left([\mathrm{K}] - \omega^2[\mathrm{M}]\right)\{\mathrm{U}\} = \{\mathrm{F}\}$, where ω is the angular frequency, $[\mathrm{K}]$ and $[\mathrm{M}]$ are the stiffness and mass matrices, respectively, and $\{\mathrm{U}\}$ and $\{\mathrm{F}\}$ are the nodal displacement and force vectors, respectively, of the unit cell. Since the origami structures analyzed in this study are periodic in the x direction with the spatial period L as shown in Figs. 1 and 2, the Bloch theorem leads to the conditions:

$$\mathbf{u}(\mathbf{r}_L) = \mathbf{u}(\mathbf{r}_0)e^{ikL}; \tag{3}$$

for the displacements on the opposite boundaries of the unit cell, assumed to lie at $x = 0$ and $x = L$, where $\mathbf{r}_0$ is the position vector of a generic point on the boundary $x = 0$ of the unit cell and $\mathbf{r}_L$ is the position vector of the correspond-

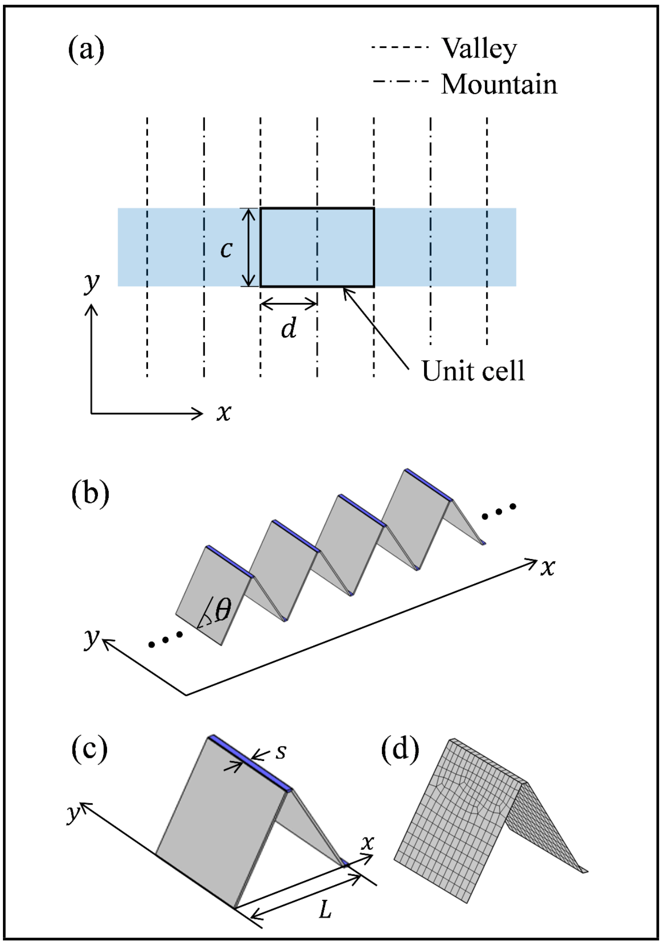

Figure 2. The schematics of (a) the folding pattern of Jabara-ori, (b) the strip-like waveguide structure considered in this study, (c) its unit cell and (d) the finite element model.

ing point on the boundary $x = L$. Applying the above relations for the nodal displacements and a similar relation for the nodal forces on the boundaries $x = 0$ and $x = L$, the governing equations are reduced to a homogeneous system of linear equations for the nodal displacement vector with a reduced degree of freedom. The condition for this system of equations to have a nontrivial solution yields the angular frequencies ω for a given Bloch wavenumber k, i.e, the dispersion relation of elastic waves. The dispersion relation of a periodic structure is also periodic in the wavenumber space and its primitive unit is called the first Brillouin zone. The first Brillouin zone corresponds to $-\pi/L \leq k \leq \pi/L$ in the one-dimensional case with the spatial period L analyzed here, but it suffices to consider its half, i.e., $0 \leq k \leq \pi/L$. The nodal displacement vector satisfying the system of equations with the so-determined ω gives the corresponding vibration mode.

In the present study, a commercial finite element analysis software COMSOL Multiphysics was used to perform the above analysis. The finite element models of the unit cells were constructed using shell elements in accordance with the Mindlin-Reissner plate theory accounting for the transverse shear and rotary inertia effects.[17] The dimensions of the unit cells assumed in the analysis were $a = b = 100$ mm and $\alpha = 60°$ for the Miura-ori structure and $c = d = 100$ mm for the Jabara-ori structure. For both Miura-ori and Jabara-ori structures, the panel thickness was set as $h = 2$ mm, and three different crease interphase widths $s = 2.5$, 5 and 10 mm were considered, corresponding to 1/40, 1/20 and 1/10 of the edge lengths of the unit cells, respectively. For each of the Miura-ori and Jabara-ori structures, four types of numerical models were analyzed corresponding to different crease interphase materials and widths as shown in Table 1. Among the four types considered here, Type I provides the reference, consisting of aluminum panels connected via polymer (nylon) crease interphase regions. Compared to Type I, Types II and III have smaller and larger crease interphase widths, respectively, with the same material properties. Type IV has the panels and crease interphase regions both made of aluminum. The assumed values for the density, Young's modulus and Poisson's ratio of aluminum were $\rho_{Al} = 2700$ kg/m^3, $E_{Al} = 70$ GPa, and $\nu_{Al} = 0.33$, respectively, and those of nylon were $\rho_{nylon} = 1150$ kg/m^3, $E_{nylon} = 2$ GPa, and $\nu_{nylon} = 0.4$, respectively. The parameters of nylon and aluminum were used for the crease interphase as representatives of soft and stiff interphases, respectively.

Table 1. Four types of origami structures.

	Type I	Type II	Type III	Type IV
Panel material	Aluminum	Aluminum	Aluminum	Aluminum
Crease material	Nylon	Nylon	Nylon	Aluminum
Crease width	5 mm	10 mm	2.5 mm	5 mm

The unit cells were discretized with 2428 triangular elements at maximum for the Miura-ori structures and with 677 rectangular elements for the Jabara-ori structures. Representative finite element models are shown in Fig. 1(d) and Fig. 2(d). The maximum size of the elements was kept smaller than 8 mm for both the panels and the crease interphases. The validity of the finite element models was checked for the Miura-ori structure of Type I by comparing the dispersion relations obtained with the above discretization fineness to those obtained by reducing the maximum element size to the half (4 mm) for six representative folding angles (0°, 40°, 50°, 60°, 70° and 80°). As a result, the difference between the dispersion curves by the two element divisions increased with the folding angle, and the maximum difference was 0.013 kHz for the folding angle of 80° at the edge of the Brillouin zone ($k = \pi/L$) of the fourth branch as far as the first to the fifth branches were concerned, which was judged acceptable for the purpose of the present analysis.

3.2. Analysis of Wave Transmission Through Finitely Periodic Origami Structures

The Bloch wave analysis outlined above provides the dispersion relation of elastic waves in the infinitely extended perfectly periodic structures. In order to supplement this analysis and gain insight into the wave transmission characteristics in a more realistic situation, the response of finitely periodic origami structures subjected to time-harmonic excitation is also analyzed. For this purpose, the Miura-ori and Jabara-ori structures of Type I and the folding angle of 60° were selected. The computational models consisted of ten unit cells of the origami structures which were embedded between strip plates as schematically shown in Fig. 3. Since crease interphase regions were arranged at both interfaces between the origami structure and the strip plates, the finite origami structures occu-

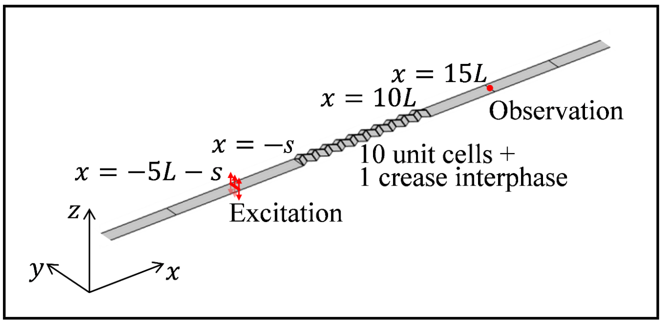

Figure 3. A schematic illustration of the finitely periodic origami structure embedded between strip plates.

pied the region $-s < x < 10L$, where L is given in Eq. (1) or Eq. (2). The strip plates were modeled with the same thickness and width as the origami structures, i.e., the thickness of 2 mm and the widths of 140 mm and 100 mm for the Miura-ori and Jabara-ori structures, respectively, and their length was set as $110L$. The same density and elastic properties as the panels of the unit cells were used for the strip plates.

The wave motion was excited by applying a time-harmonic forced displacement in the z direction u_z uniformly in the y direction at $x = -5L - s$ on one of the strip plates. The wave transmission across the origami structure was analyzed in the frequency domain by aid of the COMSOL Multiphysics software using shell elements, and the displacement components u_x, u_y and u_z were recorded at the center of the other strip plate at $x = 15L$ as functions of the excitation frequency in the range of 0.005 to 1 kHz. Both ends of the connected strip plates at $x = 120L$ and $x = -110L - s$ were assumed to be clamped. In order to suppress the reflection at these ends, the following treatment was employed in the present analysis since the so-called perfect matching layer option, commonly used to simulate non-reflecting boundaries, was not available in the COMSOL Multiphysics for shell elements. Namely, the parts of the connected strip plates farther than $10L$ away from the origami structure were modeled as a viscoelastic material with the complex-valued stiffness tensor C of the form $\mathrm{C} = \{1+i\eta(x)\}\mathrm{C}_0$, where C_0 is the stiffness tensor of the panels of the origami structure and $\eta(x)$ is a position-dependent artificial damping parameter which increases from 0 to 1 in proportion to the fourth power of the distance, $|x - 20L|$ for $x > 20L$ and $|x + 10L + s|$ for $x < -10L - s$.

4. RESULTS AND DISCUSSION

4.1. Dispersion Relations

The dispersion relations of the Miura-ori structures of Types I-IV are shown in Fig. 4 for different folding angles up to the frequency of 1 kHz. It can be observed in Fig. 4 that there are frequency ranges with no branches, i.e., elastic wave bandgaps, in which the wave propagation is prohibited in the periodic structure. The main attention in this study is paid to the bandgaps lying at relatively low frequencies since they are often of primary concern. In most of the cases shown in Fig. 4, the first (lowest-frequency) bandgap exists between the fourth and fifth branches. The location and width of this bandgap are different for different folding angles. For example, for Type I shown in Fig. 4(a), the first bandgap exists between 0.23 and 0.41 kHz (width 0.18 kHz) for $\theta = 30°$, between 0.17 and 0.58 kHz (width 0.41 kHz) for $\theta = 60°$, and between 0.26 and 0.47 kHz (width 0.21 kHz) for $\theta = 80°$, i.e., the bandgap becomes wider as the folding angle is increased from 30° to 60° but then narrower as the folding angle is further increased to 80°. The bandgap location and width are also influenced by the crease interphase width and material properties. As a general trend, Type II (wider crease interphase) shows narrower bandgaps located at lower frequencies while Type III (narrower crease interphase) shows wider bandgaps located at higher frequencies as compared to Type I. Furthermore, Type IV (stiffer crease interphase material) has the bandgap at higher frequencies as compared to Type I. It is noted as an exception that for Type IV with the folding angle of 80°, there is no bandgap between the fourth and fifth branches and the first bandgap lies above the sixth branch.

The corresponding dispersion relations of the Jabara-ori structures are shown in Fig. 5. Like the Miura-ori structures, the first bandgap exists between the fourth and fifth branches for Types I–III. It is also observed by comparison of Types I–III that the location and width of this bandgap depend on the folding angle as well as the crease interphase width, but the trend of dependence is less clear as compared to the results for the Miura-ori structures. It is noted that for Type IV with the stiffer crease interphase material, the pair of branches to open the first bandgap is dependent on the folding angle: namely, it is located between the fourth and fifth branches for $\theta = 30°$, but for $\theta = 60°$ and 80°, it is located between the third and fourth branches.

4.2. Vibration Modes: Miura-Ori Structure

Taking advantage of the plate modeling employed in this study, the vibration modes at low frequencies as well as at bandgap edges are examined for the representative model of Type I for the Miura-ori and Jabara-ori structures. First, for the Miura-ori structure at the folding angle of $\theta = 30°$, the vibration modes of the four branches at a sufficiently low frequency of 0.02 kHz are shown in Fig. 6. In Fig. 6, the first branch is dominated by the u_z displacement component. The second and third branches are both associated with the rotational motion around the x-axis, while the second branch is also accompanied by the u_y displacement. The fourth branch is dominated by the u_x displacement and also accompanied by a significant angle change at the mountain fold meandering in the x direction.

The vibration modes at the upper and lower edges of the bandgap between the fourth and fifth branches are shown in Fig. 7 for the folding angles of $\theta = 30°$ and 60°. In Fig. 7(a), the indices V1, V2, ... and E1, E2, ... are allocated to the vertices and edges of the unit cell for the ease of the following discussion. In Fig. 7(a) and (b) for the upper edge of the bandgap, the difference of the vibration modes at the folding angles of 30° and 60° can be observed clearly. Namely, in Fig. 7(a) for $\theta = 30°$, the vertices V1 and V3 show the displacement u_z in phase, while in Fig. 7(b) for $\theta = 60°$, these vertices do not show the u_z displacement but the panel edges E1 and E2 are bent in antiphase. In Fig. 7(c) and (d) for the lower edge of the bandgap, the u_z displacement is concentrated near the vertex V2 at the edge of the valley crease at $\theta = 30°$, while it

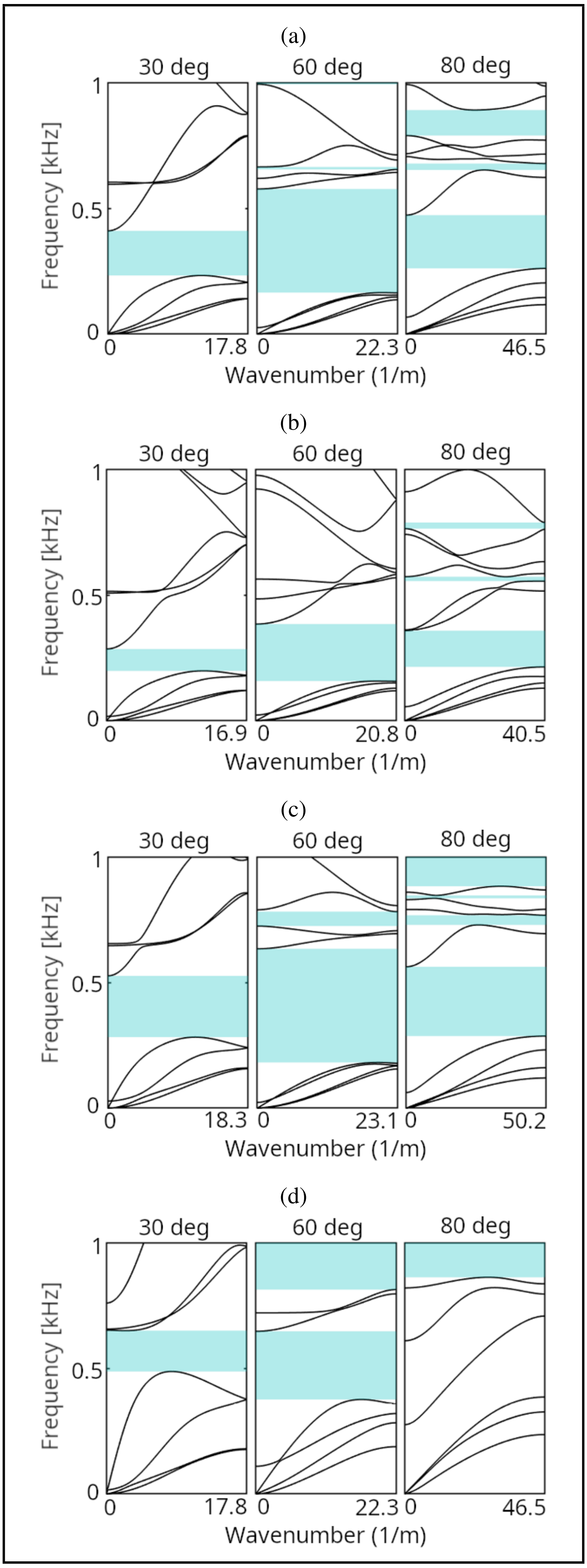

Figure 4. The dispersion relations of the Miura-ori structures of (a) Type I, (b) Type II, (c) Type III and (d) Type IV, for the folding angles of 30°, 60° and 80°. The wavenumber spans the range $0 \leq k \leq \pi/L$ in all diagrams. The bandgaps are indicated in light blue.

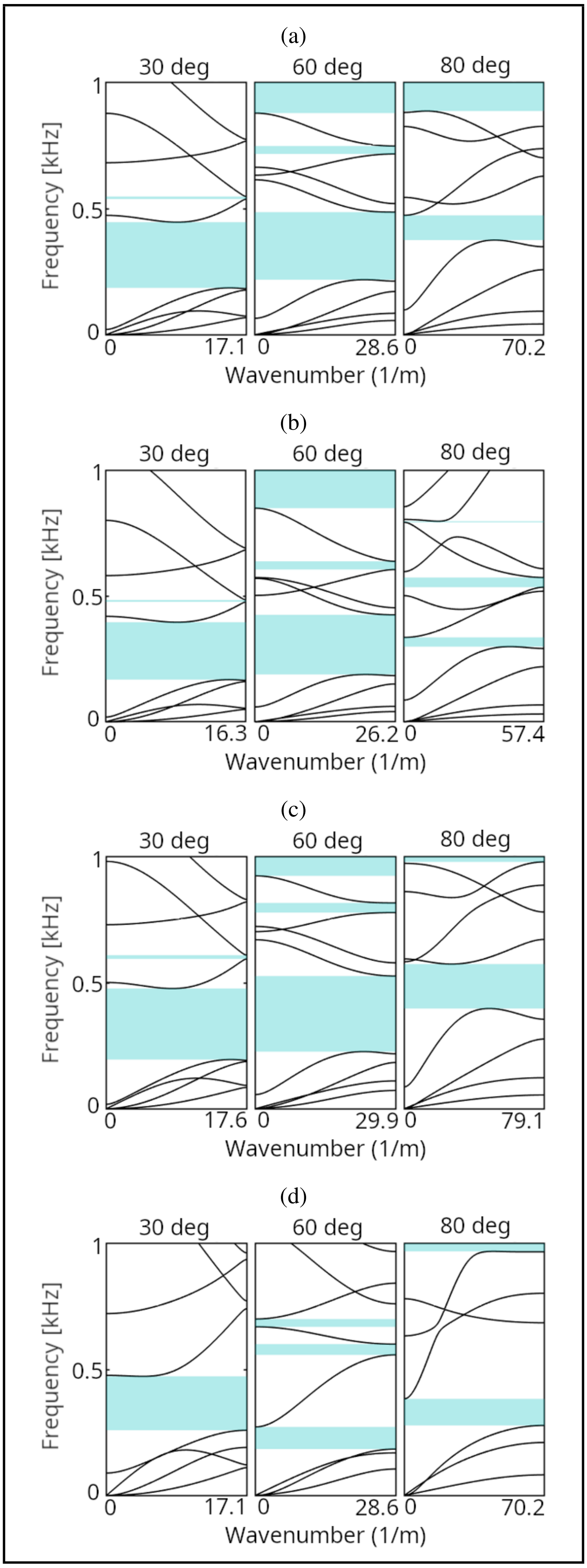

Figure 5. The dispersion relations of the Jabara-ori structures of (a) Type I, (b) Type II, (c) Type III and (d) Type IV, for the folding angles of 30°, 60° and 80°. The wavenumber spans the range $0 \leq k \leq \pi/L$ in all diagrams. The bandgaps are indicated in light blue.

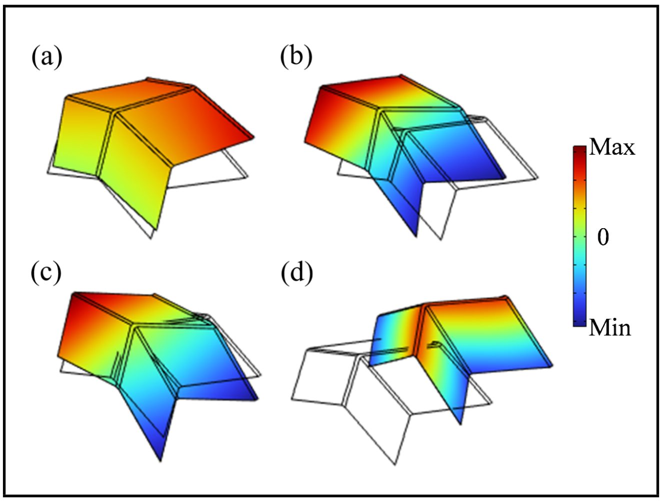

Figure 6. The vibration modes of the Miura-ori structure of Type I at the folding angle of 30° for (a) the first branch, (b) the second branch, (c) the third branch and (d) the fourth branch at the frequency of 0.02 kHz. The color corresponds to the displacement in the z direction.

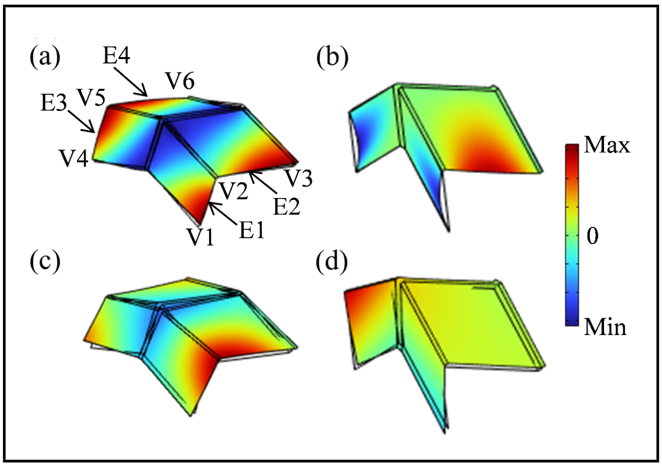

Figure 7. The vibration modes of the Miura-ori structure of Type I at the folding angles of (a) 30° (0.41 kHz) and (b) 60° (0.58 kHz) for the upper edge, and (c) 30° (0.23 kHz) and (d) 60° (0.17 kHz) for the lower edge, of the bandgap. The color corresponds to the displacement in the z direction.

is concentrated near the vertex V5 on the opposite edge of the mountain crease at $\theta = 60°$. The variation of the character of vibration modes with the folding angle is discussed further in Section 4.4 together with the folding-angle dependence of the bandgap width.

4.3. Vibration Modes: Jabara-Ori Structure

For the Jabara-ori structure at the folding angle of $\theta = 30°$, the vibration modes of the four branches at 0.02 kHz are shown in Fig. 8. At this low frequency, the first to fourth branches are dominated or associated with the u_z displacement, the u_y displacement with localized panel bending, the u_x displacement and the rotation around the x-axis, respectively. Due to the geometrical symmetry of the Jabara-ori structures with respect to the center line along the x axis, the vibration modes can be classified into symmetric or antisymmetric modes with respect to this center line in terms of the distribution of the u_z displacement. In Fig. 8, the first and third branches are associated with symmetric motions while the second and fourth branches are associated with antisymmetric ones.

The vibration modes at the edges of the bandgap between the fourth and fifth bandgap are shown in Fig. 9 for the folding angles of $\theta = 30°$ and 60°. For the upper edge of the bandgap, the vibration modes in Fig. 9(a) and (b) are similar in the sense that they both accompany flexural deformation of the panels which is symmetric with respect to the center line and the two panels in the unit cell move out of phase. The vibration modes at these folding angles are also similar at the lower edge of the bandgap as shown in Fig. 9(c) and (d) in the sense that the deformation is antisymmetric with respect to the center line and the two panels in the unit cell move out of phase.

For the Jabara-ori structures considered in this study, the bandgap formation mechanism can be discussed in the light of the above-mentioned symmetry of the vibration modes. In Fig. 10, the dispersion relations of the Jabara-ori structure of Type I are shown for the flat state of $\theta = 0°$ and for a small folding angle of $\theta = 4°$, together with the vibration modes at some representative points. At $\theta = 0°$ in Fig. 10(a), the symmetric modes can be characterized as longitudinal and flexural modes, while the antisymmetric modes as in-plane rotational and torsional modes. In this flat state, the flexural mode forms a bandgap between 0.23 kHz (the point denoted as F2 in Fig. 10) and 0.43 kHz (F3) due to the Bragg reflection. When the structure is slightly folded to $\theta = 4°$, the flexural mode is coupled with the longitudinal mode and shifts the lower edge of the bandgap down to 0.18 kHz (S1) as shown in Fig. 10(b), resulting in a broader bandgap for the symmetric modes. This behavior has been observed in the foregoing works[11,12] based on the beam models. In the present analysis, the antisymmetric modes, which are not accounted for in the above works, are also involved in the bandgap formation. Namely, the torsional mode forms a narrow bandgap between 0.66 kHz (T2) and 0.69 kHz (T3) at $\theta = 0°$, but it is coupled with the in-plane rotational mode in the folded state at $\theta = 4°$ to form a broader bandgap between 0.36 kHz (AS1) and 0.68 kHz (AS2) in a manner similar to the coupled longitudinal/flexural modes. The overlapping frequency range between 0.36 and 0.43 kHz thus becomes the bandgap for all modes. It is a common feature for all folding angles that the upper and lower edges of this bandgap are characterized by the symmetric and antisymmetric modes, respectively, although the strength of the coupling varies with the folding angle.

4.4. Folding-Angle Dependence of the Bandgaps

The upper and lower edge frequencies of the bandgap between the fourth and fifth branches are plotted in Fig. 11 as functions of the folding angle for the Miura-ori and Jabara-ori structures, together with those of the bandgap between the third and fourth branches existing for the Jabara-ori structure of Type IV. For the Miura-ori structures of Types I–IV, it is first seen in Fig. 11(a) that the bandgap opens at a finite folding angle, e.g., at $\theta = 14°$ for Type I. Above this threshold angle, the upper edge frequency increases while the lower edge frequency decreases with the folding angle and the bandgap width attains a maximum at a certain folding angle, as a trend of all Types I–IV. Among the four types, the widest bandgap is achieved by Type III with smaller crease interphase width at

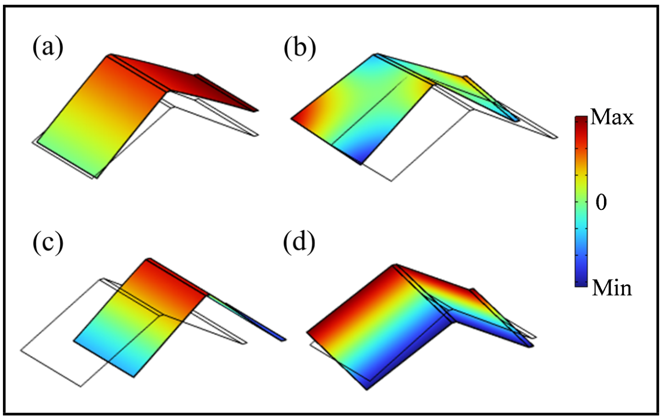

Figure 8. The vibration modes of the Jabara-ori structure of Type I at the folding angle of 30° for (a) the first branch, (b) the second branch, (c) the third branch and (d) the fourth branch at the frequency of 0.02 kHz. The color corresponds to the displacement in the z direction.

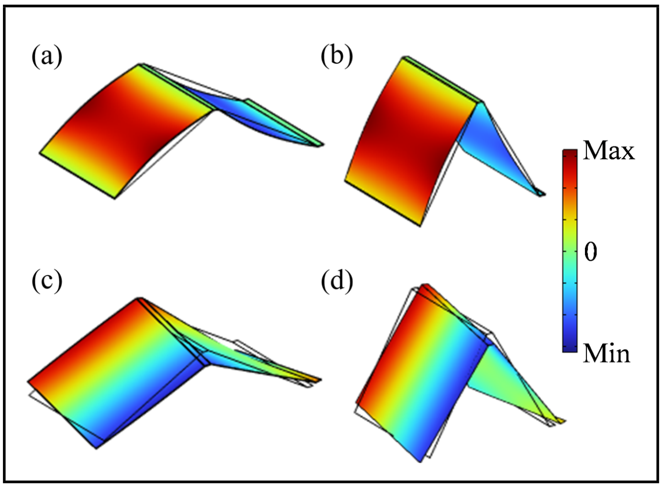

Figure 9. The vibration modes of the Jabara-ori structure of Type I at the folding angles of (a) 30° (0.45 kHz) and (b) 60° (0.49 kHz) for the upper edge, and (c) 30° (0.19 kHz) and (d) 60° (0.22 kHz) for the lower edge, of the bandgap. The color corresponds to the displacement in the z direction.

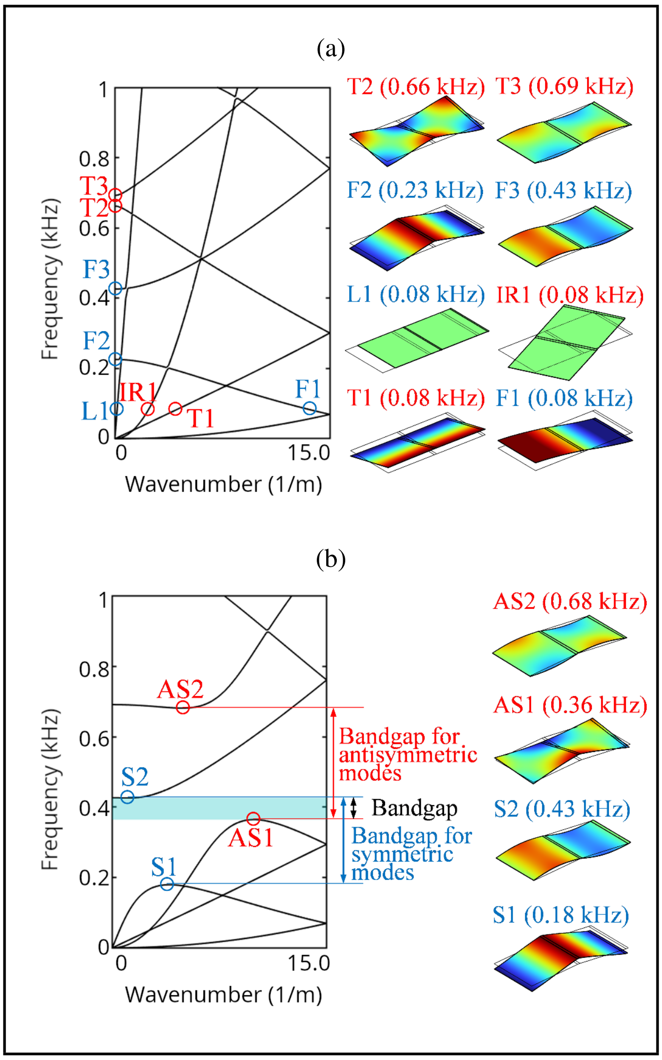

Figure 10. The dispersion relations of the Jabara-ori structure of Type I at the folding angles of (a) 0° and (b) 4°. The vibration modes are also shown for representative points on the branches corresponding to (a) longitudinal (L1), in-plane rotational (IR1), torsional (T1, T2, T3) and flexural (F1, F2, F3) motions at 0°, and (b) symmetric (S1, S2) and antisymmetric (AS1, AS2) motions at 4°. In the dispersion diagrams, the wavenumber spans the range $0 \leq k \leq \pi/L$.

$\theta = 60°$.

It has been shown in Fig. 7 for the Miura-ori structure of Type I that the vibration modes at the bandgap edges are different in character for two folding angles of 30° and 60°. At a closer examination of the folding-angle dependence of dispersion diagrams, it has been found that as θ increases from the gap-opening threshold of 14°, the fifth and sixth branches approach and touch each other at the point $k = 0$ when $\theta = 56°$ and separate away beyond this angle. Namely, the vibration modes of the fifth branch switch in character at this angle. This angle corresponds to the corner-like point of the upper edge frequency in Fig. 11(a), across which the folding-angle dependence changes from increasing to decreasing behavior. For the lower edge frequency, the switching of the vibration modes has also been observed between the third and fourth branches at an intermediate folding angle. Correspondingly, the folding-angle dependence of the lower edge frequency changes from decreasing to increasing behavior as shown in Fig. 11(a), but in a more gradual manner in contrast to the upper edge frequency.

The bandgap features of a similar Miura-ori-based strip structure have been demonstrated by Pratapa et al.[9] based on a bar-hinge model. For the structure with optimized parameters, they reported that the first bandgap was between the fourth and fifth branches, whose width attained the maximum at the folding angle of 68.64°. Qualitatively, the trend of their result is similar to the features described above. In their result, the upper edge frequency of the bandgap varied remarkably with the folding angle, while the variation of the lower edge frequency was relatively small. In contrast, both the upper and lower edge frequencies vary with the folding angle significantly in the present results. This difference is likely due to the complex deformation modes of the panels which are captured in the analysis based on the plate theory.

The folding-angle dependence of the bandgaps for the Jabara-ori structures is shown in Fig. 11(b). For the bandgap between the fourth and fifth branches, the folding angles for the gap opening are nearly zero in contrast to those of the Miura-ori structures. For Types I-IV, the upper edge frequency of this bandgap increases only gradually over a wide range of the folding angle, while the lower edge frequency exhibits a remarkable decreasing-increasing variation with the folding angle. It is also observed that Types I-III show similar variation of the lower edge frequency with the folding angle, indicating its insensitivity to the crease interphase width.

It has been shown for Type I in Fig. 9(a) and (b) that the vibration modes at the upper edge of the bandgap between the fourth and fifth branches are such that the two panels in the unit cell move out of phase. This implies that the angles between the neighboring panels do not vary so remarkably, which can explain the above-mentioned feature that the upper edge frequency is relatively insensitive to the folding angle and the crease interphase width. On the other hand, at the lower edge of the bandgap, the vibration modes are associated with antisymmetric bending of the two panels as shown in Fig. 9(c) and (d). It is likely that the influence of the folding angle on such complex deformation behavior is behind the remarkable folding-angle dependence of the lower edge frequency shown in Fig. 11(b).

For Type IV with stiffer crease interphase, the lower edge frequency of this bandgap is shifted to higher frequency and the bandgap closes at $\theta = 62°$. For this type, there is another bandgap between the third and fourth branches for the folding angles above $\theta = 44°$. It is seen that its lower edge frequency follows a similar curve to those of the bandgap between the fourth and fifth branches of Types I-III. It is also noted that among the four types, the widest bandgap is found for Type III at the folding angle of 46°.

The wave propagation in similar zig-zag structures has been studied by Nanda and Karami[11] and Xu et al.[12] using beam theories. Since their models involve the longitudinal motion and the flexural motion in a single transverse direction of the beam, at most two branches existed below the first bandgap in their analysis, in contrast to the presence of three or four branches for the Jabara-ori structures in the present analysis. In the results obtained by Nanda and Karami,[11] the upper edge frequency of the first bandgap showed a gradual increase with the folding angle, which is a trend qualitatively similar to that of the present analysis. The lower edge frequency in their analysis exhibited more remarkable and monotonically decreasing variation with the folding angle, which does not conform with the decreasing-increasing variation observed in the present analysis. The similarity and the discrepancy between their analysis and the present study can be explained by the results of the present study as shown in Fig. 9 that while the upper edge of the bandgap is associated with symmetric motions, the lower edge is associated with antisymmetric motions which are not reproducible in the analysis based on the beam theory.

The results in Fig. 11 show that the bandgap width of the Miura-ori and Jabara-ori structures can be varied significantly by their folding angle. This is a unique feature of the origami structures considered here as acoustic metamaterials. Namely, while elastic waves can be transmitted in the structure in the flat state or at small folding angles, they can be stopped for a wide frequency range when the structure is folded at a proper angle. Such tunable or programmable nature of origami structures[8–12] can be utilized for the elastic wave manipulation to enhance or suppress structural vibration and sound radiation[18] in a sophisticated manner. In the present analysis, it has also been shown that the maximum width of the bandgap and the corresponding folding angle depend on the width and material properties of the crease interphase regions. This fact indicates that a proper design of the crease regions or the panel joints in actual origami structures is necessary to achieve effective tunability of the bandgap.

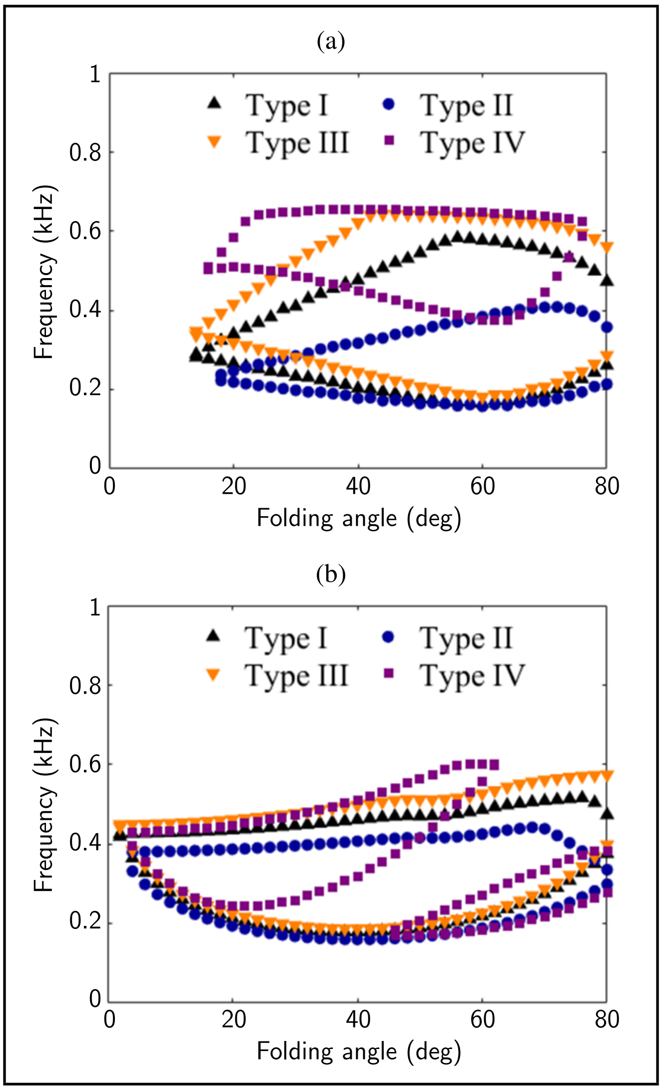

Figure 11. The folding-angle dependence of the upper and lower edge frequencies of the bandgaps for (a) Miura-ori and (b) Jabara-ori structures.

4.5. Wave Transmission Through Finitely Periodic Origami Structures

Finally, the wave transmission characteristics through the finitely periodic origami structures are examined. For the Miura-ori and Jabara-ori structures of Type I and the folding angle of 60°, the amplitudes of the transmitted wave obtained by the analysis described in Section 3.2 are plotted in Fig. 12 as functions of the excitation frequency, where they are normalized by the excitation amplitude A applied at $x = -5L - s$. In Fig. 12, the transmission spectra of the finite structures are arranged next to the dispersion diagrams of the corresponding perfectly periodic structures shown in Figs. 4(a) and 5(a). Furthermore, the distribution of $\Re[u_z]$ on the strip structures are shown for representative frequencies lying in the pass bands as well as in the bandgaps.

For the Miura-ori structure, Fig. 12(a) shows that the wave

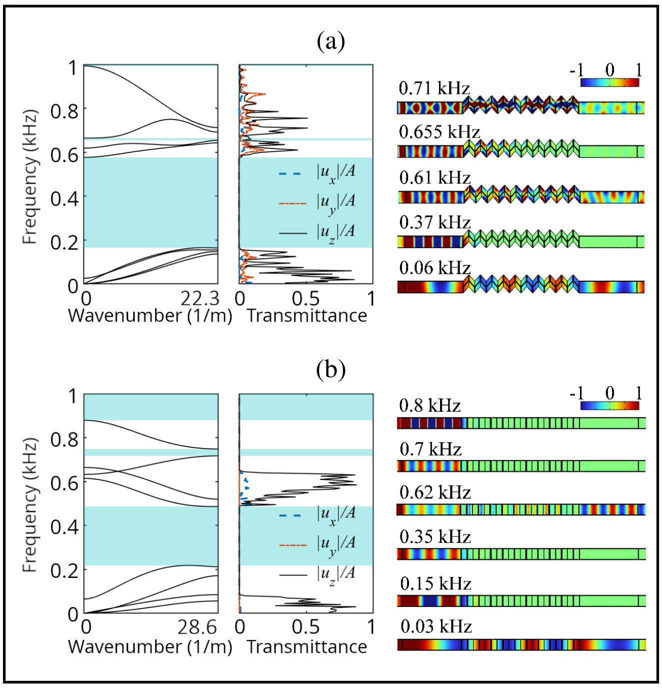

Figure 12. The frequency dependence of the normalized displacement amplitudes of the transmitted wave together with the distribution of $\Re[u_z]$ at representative frequencies and the corresponding dispersion relations for (a) Miura-ori and (b) Jabara-ori structures of Type I at the folding angle of 60°.

transmission is highly correlated with the dispersion curves of the corresponding periodic structure. Namely, the amplitudes of the transmitted wave are vanishingly small in the frequency range corresponding to the bandgap (0.17 to 0.58 kHz) between the fourth and fifth branches of the periodic structure, indicating that the wave transmission is also suppressed in finitely periodic structures in the bandgaps of the periodic structures. There is another narrow bandgap between 0.65 and 0.66 kHz for the periodic structure, where the amplitude of the u_z displacement in the finite structure drops to a few percent of the excitation amplitude. In the pass bands where the periodic structure has at least one branch, the wave is observed to be transmitted to a certain extent mainly with the u_z displacement which oscillates with the excitation frequency.

The role of the bandgaps in suppressing the wave transmission is also confirmed for the Jabara-ori structure shown in Fig. 12(b). The transmitted wave amplitudes are essentially zero in the bandgaps of the corresponding periodic structure, i.e., between 0.22 and 0.49 kHz, between 0.72 and 0.75 kHz and above 0.88 kHz. For this structure, however, the wave transmission is prohibited in wider ranges of frequency, i.e., between 0.09 and 0.49 kHz and above 0.66 kHz. This is due to the symmetry of the Jabara-ori structure with respect to the center line as already mentioned above. Namely, the branches lying between 0.09 and 0.22 kHz (third and fourth branch), between 0.66 and 0.72 kHz (seventh branch) and between 0.75 and 0.88 kHz (eighth branch) are associated with the vibration modes which are antisymmetric with respect to the center line of the structure, as shown in Fig. 13. Therefore, these modes are not coupled to the incident wave which is excited uniformly in the y direction and has a character of symmetric modes. It is noted that this feature is not observed for the Miura-ori structure which does not have such symmetry due to its complex unit cell shape.

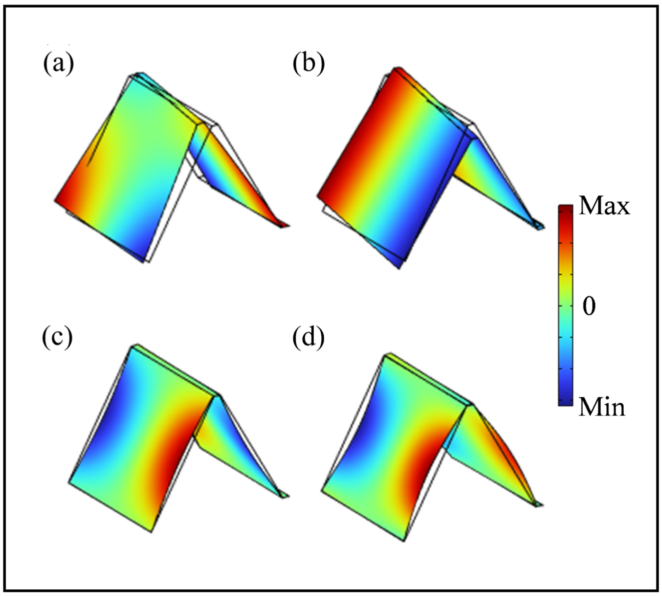

Figure 13. The vibration modes of the Jabara-ori structure of Type I with the folding angle of 60° for (a) the third branch at 0.15 kHz, (b) the fourth branch at 0.15 kHz, (c) the seventh branch at 0.7 kHz and (d) the eighth branch at 0.8 kHz. The color corresponds to the displacement in the z direction.

5. CONCLUDING REMARKS

In this study, the elastic wave bandgap features in the strip-like waveguide structures modeled on the basis of the folding patterns of the Miura-ori and Jabara-ori have been studied numerically using the finite element method. As a result, it has been shown that the features of the bandgaps in these structures, in particular the bandgap width, are highly dependent on their folding angle, thus confirming the tunable nature of their bandgaps. Owing to the plate-theory modeling, the present analysis has shown detailed features of the folding-angle dependence of the bandgaps in the light of the vibration modes of the relevant branches of the dispersion relation. The significant influence of the crease interphase parameters on the folding-angle dependence of the bandgaps found in the present analysis indicates that a proper design of the crease regions can lead to maximal tunability. Experimental verification of the computational results shown here is highly desired, and it will constitute an important subject for the future study.

It is also noted that the present study has been focused on strip-like origami structures. As a consequence, the dispersion relations have been shown only for the single direction in which the unit cells are arranged. In order to exploit the foldable properties of the Miura-ori and other types of origami, sheet-like origami structures and their two-dimensional dispersion relations (band structures) of elastic waves should be elucidated. Such an approach has already been shown based on a bar-hinge model,[9] but would desirably be taken based on plate theories for more realistic analysis.

ACKNOWLEDGMENTS

One of the authors (S. I.) acknowledges the financial support from the Mori Manufacturing Research and Technology Foundation for his post-graduate study.

DATA AVAILABILITY

The data that support the findings of this study, including the movies of the vibration modes, are openly available in the Kyoto University Research Information Repository (KURENAI) at https://doi.org/10.14989/290975.

REFERENCES

[1] Li, J., Wen, X., and Sheng, P. Acoustic metamaterials, *Journal of Applied Physics*, **129**, 171103, (2021). https://doi.org/10.1063/5.0046878

[2] Gao, N., Zhang, Z., Deng, J., Guo, X., Cheng, B., and Hou, H. Acoustic metamaterials for noise reduction: a review, *Advanced Materials Technologies*, **7**, 2100698, (2022). https://doi.org/10.1002/admt.202100698

[3] Lee, J. and Kim, Y. Y. Elastic metamaterials for guided waves: from fundamentals to applications, *Smart Materials and Structures*, **32**, 123001, (2023). https://doi.org/10.1088/1361-665x/ad0393

[4] Chen, S., Fan, Y., Fu, Q., Wu, H., Jin, Y., Zheng, J., and Zhang, F. A review of tunable acoustic metamaterials, *Applied Sciences*, **8**, 1480, (2018). https://doi.org/10.3390/app8091480

[5] Meloni, M., Cai, J., Zhang, Q., Lee, D. S. H., Li, M., Ma, R., Parashkevov, T. E., and Feng, J. Engineering origami: A comprehensive review of recent applications, design methods, and tools, *Advanced Science*, **8**, 2000636, (2021). https://doi.org/10.1002/advs.202000636

[6] Misseroni, D., Pratapa, P. P., Liu, K., Kresling, B., Chen, Y., Daraio, C., and Paulino, H. H. Origami engineering, *Nature Reviews Methods Primers*, **4**, 40, (2024). https://doi.org/10.1038/s43586-024-00328-0

[7] Filipov, E. T., Liu, K., Tachi, T., Schenk, M., and Paulino, G. H. Bar and hinge models for scalable analysis of origami, *International Journal of Solids and Structures*, **124**, 26–45, (2017). https://doi.org/10.1016/j.ijsolstr.2017.05.028

[8] Pratapa, P. P., Suryanarayana, P., and Paulino, G. H. Design of Miura-ori patterns with acoustic bandgaps. *Proc. of the ASME 2017 International Design Engineering Technical Conference & Computers and Information in Engineering Conference*, DETC2017-67384, Cleveland, Ohio, (2017). https://doi.org/10.1115/detc2017-67384

[9] Pratapa, P. P., Suryanarayana, P., and Paulino, G. H. Bloch wave framework for structures with nonlocal interactions: Application to the design of origami acoustic metamaterials, *Journal of the Mechanics and Physics of Solids*, **118**, 115–132, (2018). https://doi.org/10.1016/j.jmps.2018.05.012

[10] Han, H., Sorokin, V., Tang, L., and Cao, D. Origami-based tunable mechanical memory metamaterial for vibration attenuation, *Mechanical Systems and Signal Processing*, **188**, 110033, (2023). https://doi.org/10.1016/j.ymssp.2022.110033

[11] Nanda, A. and Karami, M. A. Tunable bandgaps in a deployable metamaterial, *Journal of Sound and Vibration*, **424**, 120–136, (2018). https://doi.org/10.1016/j.jsv.2018.03.015

[12] Xu, Z. L., Xu, S. F., and Chuang, K. C. Coupled flexural-longitudinal waves in an origami metamaterial with uncoupled creases, *Physics Letters A*, **396**, 127232, (2021). https://doi.org/10.1016/j.physleta.2021.127232

[13] Ishihara, S. and Biwa, S. Elastic wave propagation in origami-based periodic strip structures, *Proc. of the 28th International Congress on Sound and Vibration*, No. 285, Singapore, (2022). http://hdl.handle.net/2433/291283

[14] Miura, K. Method of packaging and deployment of large membranes in space, The Institute of Space and Astronautical Science Report 618, (1985). https://jaxa.repo.nii.ac.jp/records/31382

[15] Han, H., Tang, L., Cao, D., Jian, Y., and Hagedorn, P. Dynamic modeling and configuration transformation of origami with soft creases, *International Journal of Mechanical Sciences*, **285**, 109820, (2025). https://doi.org/10.1016/j.ijmecsci.2024.109820

[16] Hussein, M. I., Leamy, M. J., and Ruzzene, M. Dynamics of phononic materials and structures: Historical origins, recent progress, and future outlook, *Applied Mechanics Reviews*, **66**, 040802, (2014). https://doi.org/10.1115/1.4026911

[17] Mindlin, R. Influence of rotary inertia and shear on flexural motions of isotropic, elastic plates, *Transactions of the ASME—Journal of Applied Mechanics*, **18**, 31–38, (1951). https://doi.org/10.1115/1.4010217

[18] Liu, F., Shi, P., Shen, Y., Xu, Y., and Yang, Z. Advances in suppression of structural vibration and sound radiation by flexural wave manipulation, *Thin-Walled Structures*, **200**, 111936, (2024). https://doi.org/10.1016/j.tws.2024.111936